# Performance Improvement of an Electrothermal Microactuator Fabricated Using Ni-Diamond Nanocomposite

Li-Nuan Tsai, Guang-Ren Shen, Yu-Ting Cheng, *Member, IEEE*, and Wensyang Hsu

***Abstract*—In this paper, a low-temperature stress-free electrolytic nickel (EL) deposition process with added dispersed diamond nanoparticles (diameter $< 0.5\ \mu\mathrm{m}$) is developed to synthesize Ni-diamond nanocomposite for fabricating electrothermal microactuators. Device characterization reveals dramatic performance improvements in the electrothermal microactuator that is made of the nanocomposite, including a reduction in the input power requirement and enhanced operation reliability. In comparison with the microactuator made of pure nickel, the nanocomposite one can save about 73% the power for a 3 $\mu$m output displacement and have a longer reversible displacement range, which is prolonged from 1.8 $\mu$m to more than 3 $\mu$m. Furthermore, the nanocomposite device exhibits no performance degradation after more than 100 testing cycles in the reversible regime. The enhancements increase with the incorporation of the nanodiamond in a nickel matrix, so the Ni-diamond nanocomposite has potential for application in MEMS fabrication. [1610]**

## I. Introduction

ELECTROTHERMAL microactuators have been widely utilized for the fabrication of microgrippers [1], microswitches [2] and micromanipulators [3], with electrical, optical and biomedical applications [4]–[6]. The microactuators provide microscale mechanical movements with an electrical energy input, that is based on the thermal expansion property of a material. The device can be fabricated using existing integrated circuitry (IC) manufacturing infrastructures and processes, and so has drawn much research attention. A variety of electrothermal microactuators have been developed recently [7]–[9]. Some of the devices have been made of polysilicon using silicon-based micromachining processes [10], [11] and others are made of electroplated metal. Metal-based electrothermal microactuator has several advantages over polysilicon-based one: they can provide a larger output displacement with a smaller input voltage, can easily achieve thick structure by electroplating ($\sim 16\ \mu\mathrm{m/hr}$) for large output force, and can be fabricated at low temperature ($\sim 50\ ^{\circ}\mathrm{C}$) without having a high-temperature polysilicon doping step. For low-cost and CMOS-compatible applications, such metal-based technology provides an alternative means of manufacturing MEMS-based microactuators. However, the metal-based electrothermal microactuator generally suffers from mechanical deficiencies, such as fatigue and aging [14], [15]. In general, at temperatures higher than 350 °C, nickel structures will degrade and have an irreversible darkening on the surface along with the actuator stroke due to surface oxidation [16]. Although low operational temperature can effectively prevent the actuator from oxidation, it could result in poor performance including smaller output force and displacement.

In 2002, Teh *et al.* [17] proposed the incorporation of diamond nanoparticles into an electroless nickel matrix to enhance greatly the overall stiffness of the nickel film due to the extreme hardness, stiffness, and temperature resistance of the diamond particle. As more diamond nanoparticles are incorporated into the matrix, the residual stress in the composite film is reduced, making it more suitable for fabricating suspended microstructures. In comparison with the electroless plating technique, electrolytic nickel (EL) plating has been a very important fabrication technique for 3D-MEMS due to the characteristics of lower processing temperature and better process stability and controllability. Diamond has also much higher hardness and Young's modulus than the EL. They are 75 and 1050 GPa for diamond and 6.7 and 200 GPa for EL, respectively. Thus, this paper is aimed to present a newly developed CMOS-compatible electrolytic Ni-diamond nanocomposite synthesis for fabricating the electrothermal microactuators. Effects on the performance of electrothermal microactuators resulted by the incorporation of diamond nanoparticles are also further investigated in terms of the mechanical strength, coefficient of thermal expansion (CTE) of the nanocomposite material, and the improvements of power consumption and operational reliability in the devices.

## II. Characterizations of Nanocomposite Films

Before incorporating a nanocomposite material into MEMS devices, it is important to have a better understanding of the material characteristics and potential impact on device performance. To facilitate this, four kinds of as-fabricated 50 $\mu$m wide, 6 $\mu$m thick cantilevers shown in Fig. 1 are utilized for the examination of the material property enhancements in terms of static and dynamic characteristics, such as hardness and Young's modulus to density ($E/\rho$) ratio. The beam lengths are

Manuscript received June 7, 2005; revised August 30, 2005. This work is supported by the National Science Council of ROC under Grant NSC 92-2220-E-009-002, NSC 92-2212-E-009-035, and in part by MediaTek Research Center. Subject Editor C. Hierold.

L.-N. Tsai is with the Microsystems Integration Laboratory, Department of Electronics Engineering, National Chiao Tung University, Hsinchu, Taiwan 300, R.O.C., and also with the Microsystems Integration Laboratory, Department of Electronics Engineering, National Chiao Tung University, Hsinchu, Taiwan 300, R.O.C. (e-mail:ytcheng@mail.nctu.edu.tw).

G.-R. Shen and Y. T. Cheng are with the Microsystems Integration Laboratory, Department of Electronics Engineering, National Chiao Tung University, Hsinchu, Taiwan 300, R.O.C. (e-mail:ytcheng@mail.nctu.edu.tw).

W. Hsu is with the Department of Mechanical Engineering, National Chiao Tung University, Hsinchu, Taiwan, 300, R.O.C.

Digital Object Identifier 10.1109/JMEMS.2005.863737

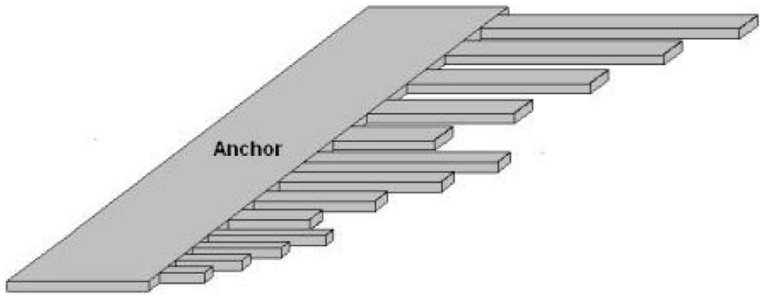


Fig. 1. Schematic diagram of cantilevers for material characterizations.

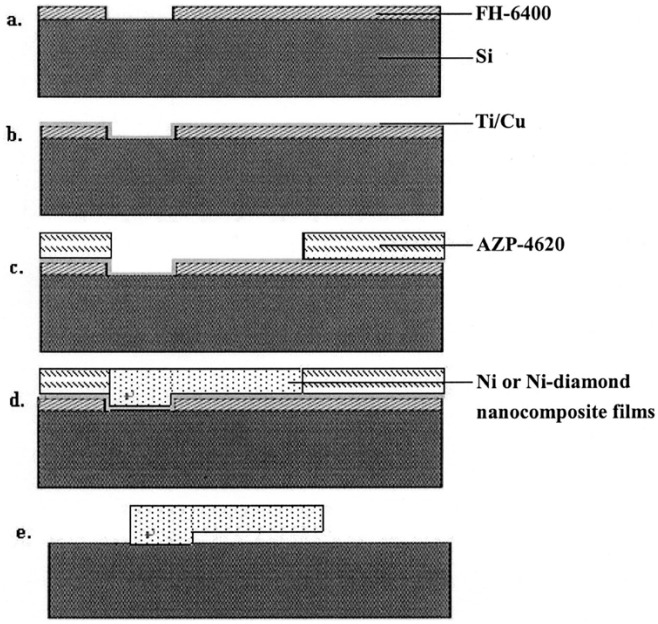


Fig. 2. Fabrication process flow of cantilevers: (a) 1 $\mu$m FH-6400 PR deposition and patterning. (b) sputtered Ti/Cu (100 Å/1000 Å) as an adhesion and seed layer. (c) 10 $\mu$m AZP-4620 PR deposition and patterning as the molding structure. (d) electrolytic nanocomposite plating. (e) structure releasing.

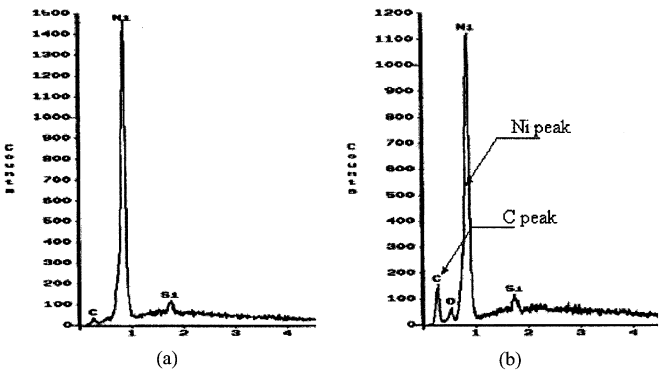


Fig. 3. EDS spectra of the (a) pure Ni film and (b) the nickel-diamond nanocomposite film.

designed as 150 $\mu$m, 250 $\mu$m, 350 $\mu$m, and 450 $\mu$m, respectively. Fabrication of the cantilevers is schematically illustrated in Fig. 2. The fabrication starts with a 1 $\mu$m thick photoresist (PR) deposition, which is patterned as a sacrificial layer on a 4" n-type silicon substrate [see Fig. 2(a)]. A thin 100 Å Ti/1000 Å Cu film is then DC-sputter deposited as an adhesion and plating seed layer [see Fig. 2(b)]. Another 7 $\mu$m PR is coated and patterned to form the electroplating mold [see Fig. 2(c)] and electrodeposition of Ni or Ni-diamond nanocomposite is performed to construct the structural layer of the cantilevers at 50 °C [see Fig. 2(d)]. The plating current density is controlled at 10 $\mathrm{mA/cm^2}$. Finally, the beam structures in Fig. 2(e) are then released after sequentially stripping the sacrificial layer by acetone (ACE), rinsing in isopropylalcohol (IPA) and deionized (DI) water, as well as drying by compressed air. Once the Cu seed layer underneath the released beams is removed by immersing in a diluted $H_2SO_4$ solution for 5 s, the cantilevers are completely fabricated for following material characterizations. In the experiment, the nanocomposite films are synthesized in different plating solutions, which have different weight fractions of the diamond nanoparticles ranging from 0 to 2 g/L in the nickel baths. Table I lists the composition of the nickel-plating bath used in the experiment. The average size of the added diamond nanoparticles is below 500 nm in diameter.

The composition of the electroplated nanocomposite layer is first identified by energy dispersive spectrum (EDS). Fig. 3(a) shows the EDS of the cantilever beam made of pure Ni indicating that the electroplated layer contains very little carbon (C) in addition to Ni, Si, and O, which could be attributed to surface contamination. As compared, the stronger carbon signal in the EDS of the Ni-diamond nanocomposite shown in Fig. 3(b) indicates the existence of large amount of carbon content inside the film. In order to further verify that the carbon signal is originated from the diamond nanoparticles, X-ray diffractometer (XRD), Philips X'Pert Pro (MRD), is then utilized to compare the pure Ni and Ni-diamond nanocomposite films. The X-ray source is a Cu-$k\alpha$ line with the wavelength of 0.154 nm. The detection is made at a low angle $(2\theta)$ in the range of 20° to 60°. Fig. 4(a) shows the diffraction spectra of the pure Ni film. The Ni (111) and Ni (200) peaks appear at the angles of 45° and 53°, respectively. The corresponding interlayer spacings of $d_{111}$ and $d_{200}$ are 2.012 Å and 1.725 Å, respectively. The same Ni peaks are also found in the XRD spectra of the Ni-diamond nanocomposite as shown in Fig. 4(b). In addition, the C (102) peak around $2\theta = 50.5°$ with corresponding 1.801 Å interlayer spacing indicates the existence of crystalline diamond in the composite film. Once the inclusion of nanodiamond in Ni matrix is verified, the nanocomposite films and cantilevers are used for the following mechanical property characterizations.

The hardness of the nanocomposite film is characterized by the nanoindenter [18], XP system of the America MTS Company. Fig. 5 shows the hardness increases with the concentra-

TABLE I
THE COMPOSITION OF NI PLATING BATH

| Composition | Quantity |
|---|---|
| Nickel Sulfamate, Ni $(SO_3NH_2)\cdot 4H_2O$ | 400 g/L |
| Nickel Chloride, $NiCl_2\cdot 6H_2O$ | 5 g/L |
| Boric Acid, $H_3BO_3$ | 40 g/L |
| Wetting Agent | 5 g/L |

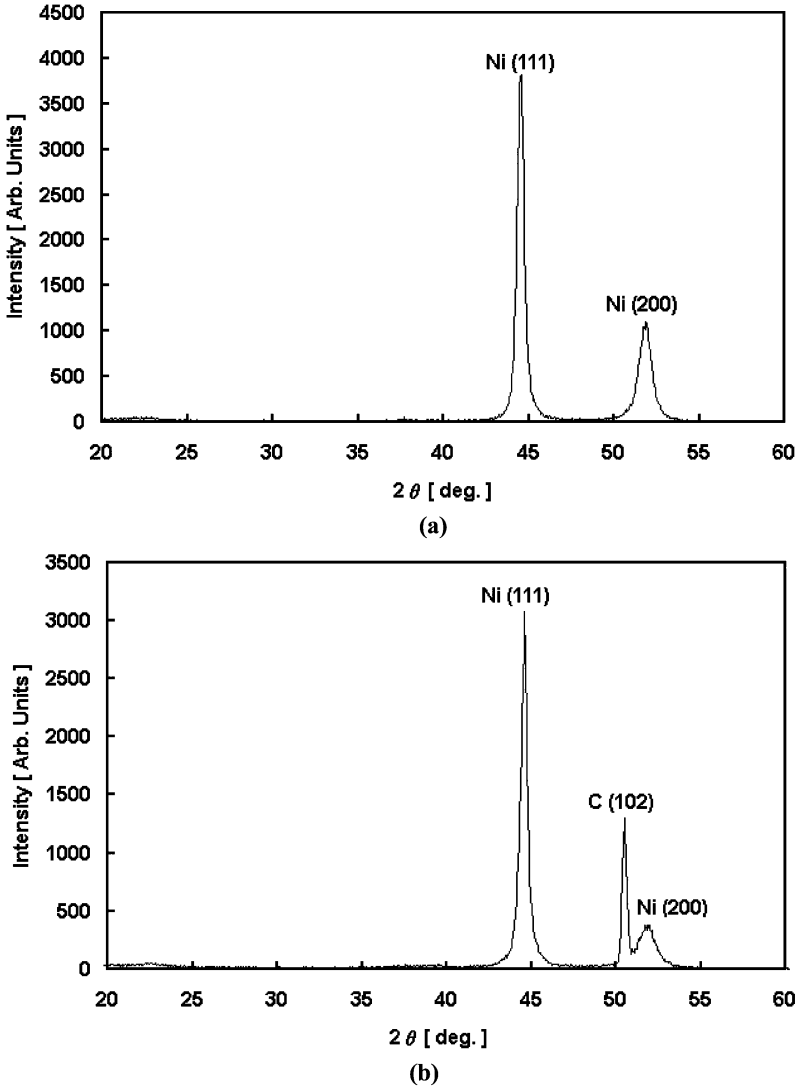


Fig. 4. X-ray diffraction spectra of the electrolytic (a) pure Ni film and (b) the nickel-diamond nanocomposite film. The carbon peak C (102) indicates the existence of diamond crystalline.

tion of the diamond nanoparticles in a plating bath. The hardness enhancement can be attributed to the incorporation of diamond nanoparticles. For the case of the nanocomposite film plated with the concentration of 2 g/L nano-diamonds, it can have 2.6 times larger hardness than the pure nickel one. On the other hand, a laser doppler vibrometer (LDV) is utilized to characterize the dynamic behavior of the electroplated films. The $E/\rho$ ratio of the films can be derived from resonant frequencies of the cantilevers that are made of the EL with different amounts of diamond nanoparticle incorporations. The relationship between $E/\rho$ ratio and resonant frequency is determined by the following (1) [19]:

$$f = 0.1615\sqrt{\frac{E}{\rho}}\left(\frac{h}{L^2}\right) \tag{1}$$

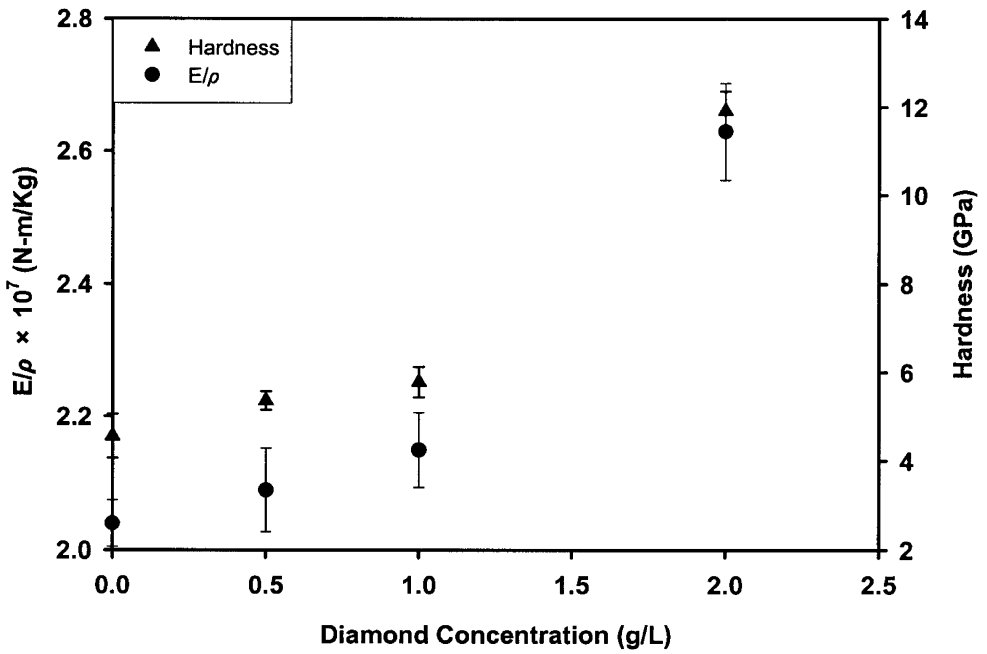


Fig. 5. Hardness and $E/\rho$ ratio of the EL films plated with various nano-diamond concentrations.

where $E$, $\rho$, $h$, and $L$ are the Young's modulus and density of the structural material and the thickness and length of the beam, respectively. Since the resonant frequency is very sensitive to the values of $h$ and $L$, process variations should be considered for the accurate calculation of $E/\rho$ ratio. Table II lists one set of frequency measurement results of 350 $\mu$m long, 50 $\mu$m wide cantilevers. The actual thicknesses of the beams plated in four different baths are 5.5 $\mu$m (pure Ni), 5.08 $\mu$m (0.5 g/L diamond), 5.06 $\mu$m (1 g/L diamond), and 4.4 $\mu$m (2 g/L diamond), respectively, instead of the original targeted 5 $\mu$m thickness. In addition, before measuring, we used Tetramethylammonium hydroxide (TMAH) to further etch away the silicon underneath the cantilevers in order to prevent the beams being stuck to the substrate during vibration. Thus, the actual beam length is typically longer than its original design due to the undercut effect as shown in Fig. 6. Part of silicon under the beam anchor is etched, so the edge of the anchor pad is freely suspended and the stiffness of the structure is reduced [20]. The undercut effect results in the underestimation of $E/\rho$ ratio. After taking both process variations into account, a more accurate $E/\rho$ ratio is extracted and listed in Table II.

The derived $E/\rho$ values corresponding to different concentration of nanodiamonds in plating bath are plotted in Fig. 5. Similar trend of hardness enhancement with increasing concentration is obtained. Total of 32 samples from eight different wafers were measured. Each data point presented is an average value obtained from the measurement of four samples on two different wafers, which were plated with the same condition but in two individual runs. The error bars represent the process variation between two identical plating conditions. The nonlinear behavior is most likely induced by process variation and can be eliminated by taking averages of more measured data. The cantilever fabricated in a plating bath with 2 g/L diamond nanoparticles has about 1.29 times higher $E/\rho$ ratio than the one made of pure nickel. The mechanical property enhancements due to the incorporation of diamond nanoparticles into nickel matrix ensure the electrolytic process for the further fabrication of electrothermal microactuators.

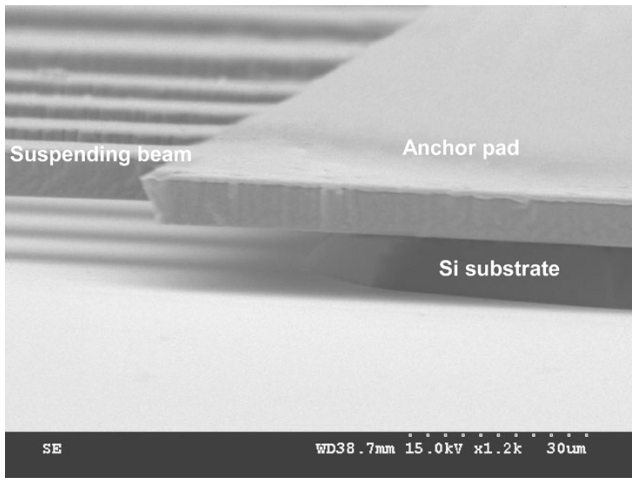


Fig. 6. Cross-sectional SEM photograph near the edge of anchor pad with the undercut effect.

## III. Design, Fabrication, and Measurement of the Electrothermal Microactuator

The electrothermal microactuator with long-short beam configuration [22] as shown in Fig. 7 is used for the experiment. The actuator has a pair of connected cantilevers that are made of the same material but with different actuating arm lengths. In the design, the two beams have a length ratio of 0.5 and a 10 $\mu$m gap spacing between them. Both beams have the same width and thickness. The longer beam is about 800 $\mu$m long, 10 $\mu$m wide, and 9 $\mu$m thick. Via electrically resistive heating of these two beams, the arm tip curls toward the side of the shorter one due to the unequal thermal expansions of two beams. Fab-

TABLE II
MEASURED FREQUENCIES OF THE DESIGNED 5 $\mu$m THICK, 350 $\mu$m LONG CANTILEVERS PLATED WITH VARIOUS NI-DIAMOND NANOCOMPOSITES

| Concentration of Diamond Nanoparticles (g/L) | Measured Beam Thickness (μm) | Effective Beam Length[1](μm) | Measured Resonant Frequency (KHz) | $E/\rho$ ratio[2] (N·m/Kg) | $E/\rho$ ratio[3] (N·m/Kg) |
|---|---|---|---|---|---|
| 0 | 5.5 | 535 | 14.031 | $3.6\text{x}10^6$ | $2.04\text{x}10^{7*}$ |
| 0.5 | 5.08 | 409 | 22.436 | $1.12\text{x}10^7$ | $2.09\text{x}10^7$ |
| 1 | 5.06 | 372 | 27.367 | $1.32\text{x}10^7$ | $2.15\text{x}10^7$ |
| 2 | 4.4 | 352 | 29.45 | $2.57\text{x}10^7$ | $2.64\text{x}10^7$ |

[1]The effective beam length is equal to the designated beam length (350 μm) plus the undercut length.
[2]Before considering the process variations.
[3]After considering the process variations.
*Typical $E/\rho$ ratio is about $2.02\text{x}10^7$ N·m/Kg (=180GPa/8908Kg/m$^3$). [21]

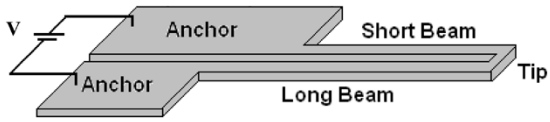


Fig. 7. Schematic diagram of the electrothermal microactuator with a long-short-beam design.

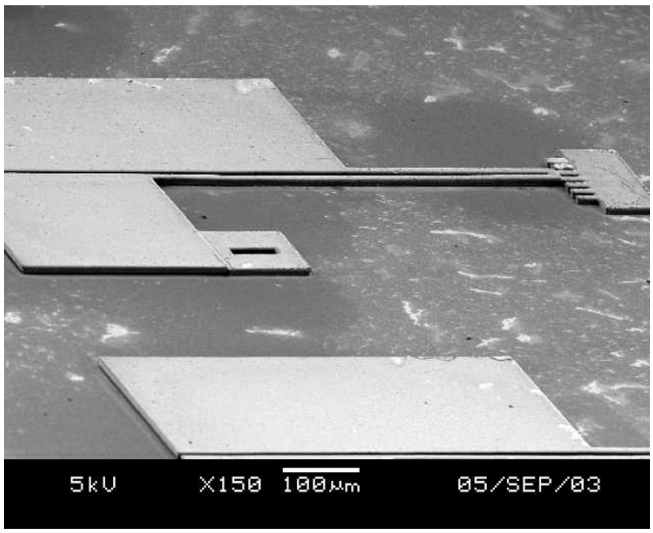


Fig. 8. SEM photograph of the fabricated electrothermal microactuator using Ni-diamond nanocomposite plated with the concentration of 2 g/L nanodiamonds.

rication of the electrothermal actuator is similar to that of the cantilevers (described in Section II) with the exception that a 2-$\mu$m $SiO_2$ film is used as a sacrificial layer instead. The sacrificial oxide layer is removed by etching it in HF solution for 10 s. A SEM photograph of the completed electrothermal actuator is shown in Fig. 8. Device testing is conducted on a probe station with an automated CCD image system with 0.2 $\mu$m resolution. Fig. 9 shows the displacement versus input power data obtained from the actuators plated in the baths with different nano-diamond concentrations. The microactuator made of the pure nickel provides a 3-$\mu$m displacement with an input power of 0.924 W. Meanwhile, the required input power for the same output displacement decreases with the concentration increase of diamond nanoparticles. It indicates that the microactuator made of nanocomposite is more efficient than the one made of pure nickel. To produce a 3-$\mu$m displacement, the microactuator made of the Ni-diamond nanocomposite plated in a bath with 2 g/L concentration of nanodiamond requires only 0.248 W, a 73% reduction in power consumption in comparison with that of a pure nickel device.

An electrothermal microactautor is normally operated in the region of reversible deformation in which the device must come back to its initial position while input power is removed. According to the actuation measurement, we found that the microactuator made of the Ni-diamond nanocomposite has a reversible output displacement over 3 $\mu$m. In comparison with the pure nickel one, which exhibits irreversible deformation once the output displacement is over 1.8 $\mu$m, the nanocomposite actuator can indeed provide a better reversible characteristic. Fig. 10 shows cycling test results. The tests are performed on both sets of actuators, which are made of the pure nickel and the Ni-diamond nanocomposite (2 g/L) films, respectively, with the operational range from 0 to 3 $\mu$m. The hysteretic displacement and surface darkening occur in the pure nickel device during the first cycling test and the device is permanently deformed even after the power is reduced to 0 W. The resting position of the deformed device is 0.2 $\mu$m away from its designed origin. In contrast, no hysteresis is found in the nanocomposite device. The back and forth displacements are almost overlapped and no degradation has been found after 100 times cycling tests. The overall results indicate that the electrothermal microactuator made of the nanocomposite not only has better power efficiency but also has enhanced operational reliability by extending the reversible displacement range of the structure.

## IV. DISCUSSIONS

The CTE measurement and ANSYS simulation are performed to investigate the effects that the nanocomposite may have on electrothermal actuator performance. Equation (2) shows an analytical relation between the output displacement

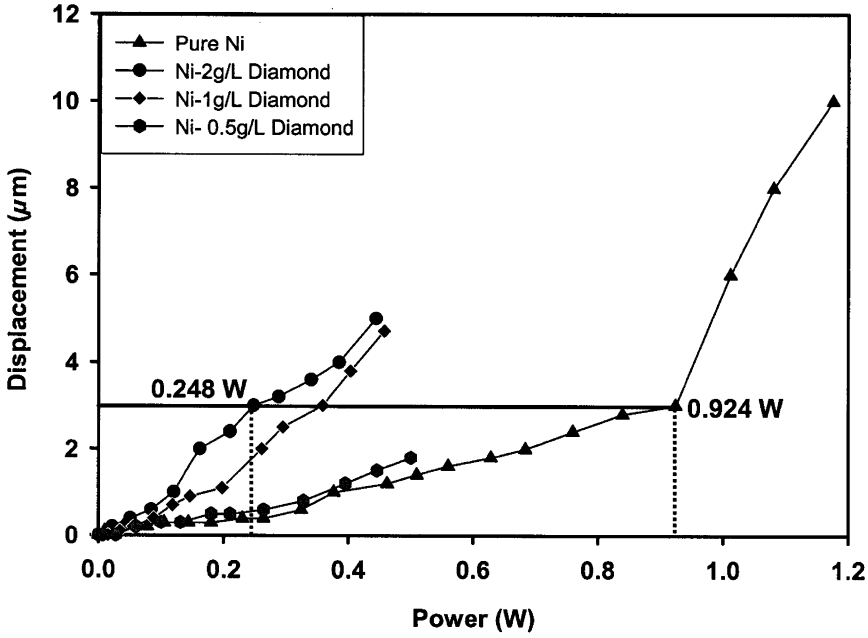


Fig. 9. Input power versus displacement of the microactuators made of the nanocomposites plated with different nanodiamond concentrations.

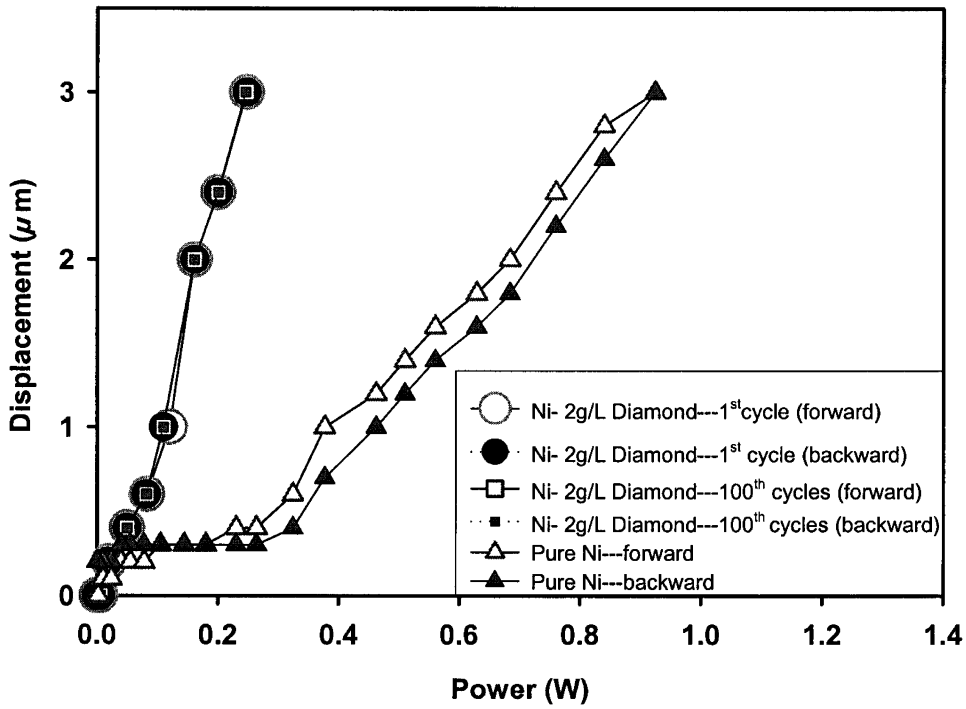


Fig. 10. Cycling tests of the microactuators made of pure Ni and the nanocomposites plated with the concentration of 2 g/L nanodiamonds.

and the CTE of the structural material of electrothermal microactuator [9]

$$\delta = \alpha(\gamma_{\text{long}} \cdot \Delta T_{\text{long}} - \gamma_{\text{short}} \cdot \Delta T_{\text{short}}) \tag{2}$$

where $\delta$ is the displacement of beam tip, $\alpha$ is the CTE, and $\gamma_{\text{long}}$, $\gamma_{\text{short}}$, $\Delta T_{\text{long}}$, and $\Delta T_{\text{short}}$ are the conversion factors and average temperature changes of the long and short beams, respectively. Since the conversion factor is only a function of the device geometry which is independent of material properties, CTE increase could be the major factor to enhance the device performance. In order to verify the supposition, an in-house apparatus shown in Fig. 11 is utilized for the CTE measurement of the electroplated Ni-diamond nanocomposite film. By measuring the elongation of cantilever in a heated chamber with temperature control, one can obtain the CTE by (3)

$$\alpha(T_1) = \frac{(L_1 - L_0)}{L_0} \cdot \frac{1}{\Delta T} \tag{3}$$

where $L_1$ is the beam length at temperature $T_1$, $L_0$ is the initial beam length at temperature $T_0$, and $\Delta T = T_1 - T_0$. Fig. 12

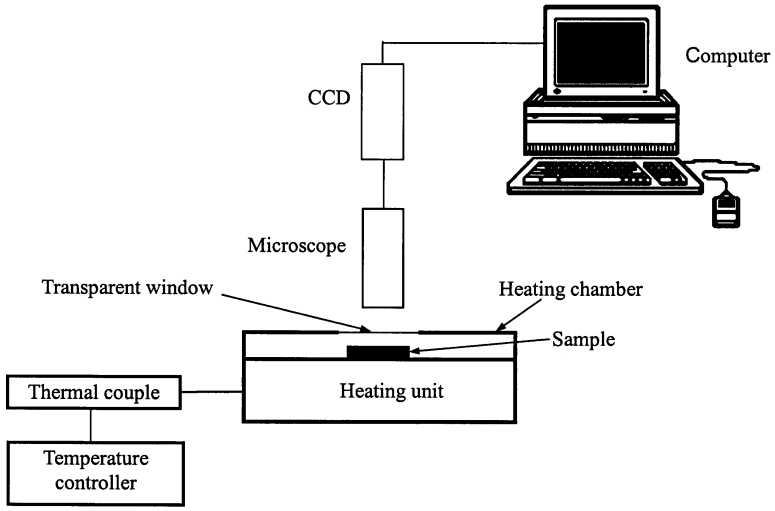


Fig. 11. Schematic diagram of the CTE measurement apparatus.

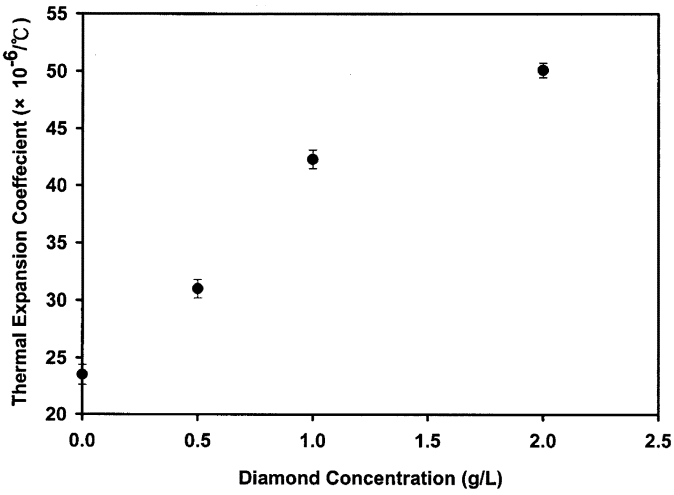


Fig. 12. CTE values of the nanocomposites plated with various nanodiamond concentrations at 400 °C.

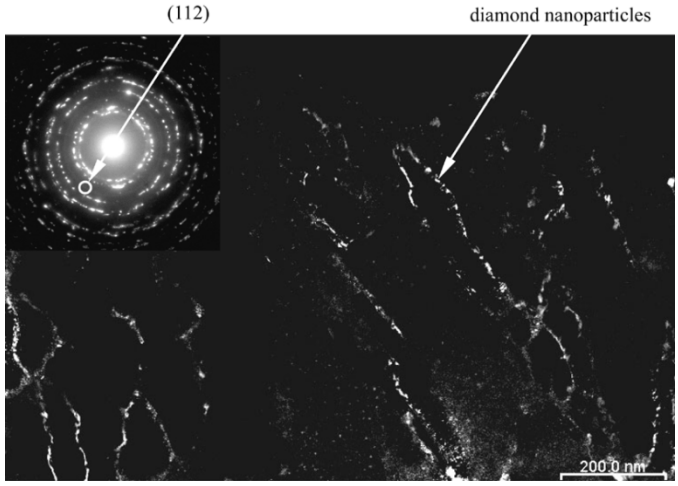


Fig. 13. Dark field TEM image of the fabricated electrolytic Ni-diamond (2 g/L) microactuator, indicating diamond nanoparticles distribute in the region of grain boundary.

shows the CTE's of the nanocomposites with different diamond nanoparticle concentrations at 400°C. The CTE value increases with the concentration of diamond nanoparticle starting from the $23 \times 10^{-6}/^{\circ}\mathrm{C}$ of pure nickel to the $50 \times 10^{-6}/^{\circ}\mathrm{C}$ of the nanocomposite plated in a bath with 2 g/L of diamond nanoparticle. That is more than two-fold of increasing in CTE values contributed by the diamond particles. Once the CTE values are determined, the commercial finite element simulator, ANSYS 6, is then utilized to simulate the electro-thermo-mechanical behavior of the microactuator in which the element type of solid 5 is applied for the analysis. TEM analysis of the nanocomposite plated with the condition of 2 g/L nano-diamond concentration was performed. Fig. 13 is a dark field image taken from the nanocomposite film and it indicates that most of the diamond nanoparticles distribute in the grain boundary regions of the nickel matrix. On the other hand, according to the elemental analyzer (EA) measurement, the diamond content of the corresponding nanocomposite film is only 0.185% in weight fraction and 0.47% in volume fraction, which are calculated based on the density of nickel ($8.908\ \mathrm{g/cm^3}$), the density of diamond particle ($3.51\ \mathrm{g/cm^3}$) and the assumption of no existence of voids inside the films. Thus, the material properties of the nanocomposite for the simulation, such as the thermal conductivity and specific heat capacitance, are assumed to be the same as that of pure nickel for the simulation due to such small amount of diamond incorporation. Meanwhile, according to the rule of the mixture [23], [24] and the previous measurement result of the $E/\rho$ ratio, the effective Young's modulus and density for the Ni-diamond nanocomposite plated in a bath with 2 g/L concentration of nano-diamond can be derived as 233.5 GPa and $8.882\ \mathrm{g/cm^3}$, respectively. Table III lists the related data about the mechanical and thermal properties of the Ni and Ni-diamond nanocomposite for finite element analysis [25], [26].

In the analysis, only conductive heat transfer mode is considered since heat convection can be neglected at moderate temperature [27], [28]. Most of the heat generated in the electrothermal actuator will be transferred to device's anchor pads or through air gap to silicon substrate by conduction mechanism. Besides, the anchors were assumed at a constant temperature 25 °C because the anchor pad is much larger than the heating element of the actuator in the design. Fig. 14 shows the simulation results.

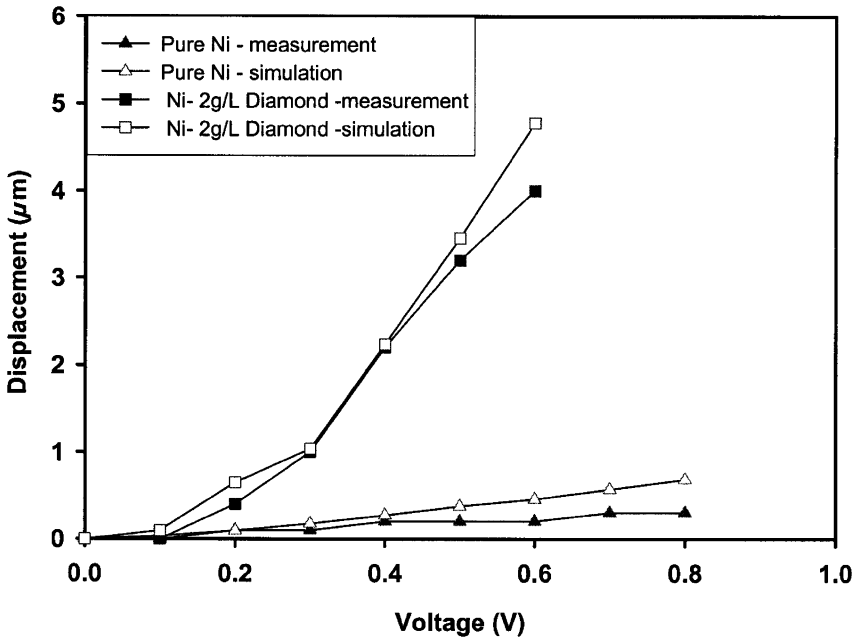


Fig. 14. Comparison of the experimental data with the ANSYS analysis in terms of the output displacements of the microactuators at different applied voltages.

TABLE III
MATERIAL PROPERTY LIST FOR ANSYS SIMULATIONS

| | Pure Ni | Ni-diamond (2g/L) |
|---|---|---|
| Modulus of Elasticity (GPa)* | 181.7 | 233.5 |
| Density (kg/m$^3$)* | 8908 | 8882 |
| Thermal Expansion Coefficient ($10^{-6}$/°C) at 400°C | 23 | 50 |
| Poisson Ratio | 0.31 | |
| Thermal Conductivity (W/mK) | 90.5 | |
| Specific Heat (J/Kg-K) | 443.08 | |
| Resisvitity (μΩ-cm) | 13.5 | |

*The data are calculated based on the rule of mixture [23,24] and the experimental results of the EA analysis and $E/\rho$ measurement.

The relation between output displacement and input voltage is closely fitted with experimental data in the low input voltage region ($< 0.4$ V), indicating that CTE has evident effect on the displacement of electrothermal microactuator. With the incorporation of diamond nanoparticles in the nickel matrix, the CTE increases as well as the output displacement of electrothermal microactuators. Regarding the deviation between the simulation and experimental results, it could be attributed to the temperature dependence of the electrical resistance of pure nickel and nanocomposite and the mentioned neglect of heat convection mechanism in the thermal analysis.

In addition to displacement, the output force of the actuator is also analyzed using ANSYS simulator with the same boundary conditions. Fig. 15 shows the comparison of the output forces between the actuators made of pure Ni and Ni-diamond nanocomposite at different input voltage. The result shows the electrothermal actuator made of Ni-diamond nanocomposite can provide larger output force than that made of pure Ni while both devices are operated with the same input voltage. Furthermore, from Figs. 9, 14, and 15 it is found that the incorporation of diamond nanoparticles into Ni matrix can enhance the output force and displacement of microactuator simultaneously. For about 0.4 V input, the actuator made of Ni-diamond nanocomposite has 2.23 $\mu$m displacement and 10 $\mu$N output force, which are larger than that made of pure Ni only with 0.27 $\mu$m displacement and 1.9 $\mu$N output force. The result infers that the nanocomposite has better energy conversion than pure Ni which is resulted by the incorporation of diamond nanoparticles. Further investigation is required.

## V. CONCLUSION

A low-temperature stress-free deposition process of the EL-diamond nanocomposite for fabricating cantilevers and electrothermal microactuators has been successfully demonstrated here. Test results indicate that the incorporation of diamond

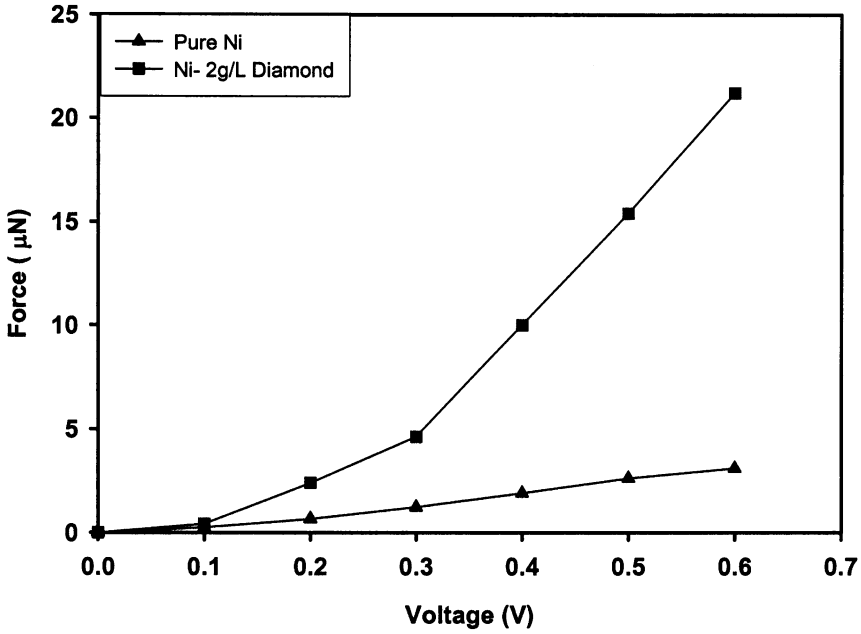


Fig. 15. Comparison of the output force of the actuators made of pure Ni and Ni-diamond nanocomposite respectively at different applied voltages.

nanoparticles effectively modifies the material properties of pure EL film, such as hardenss, $E/\rho$ ratio, and CTE, making it a more suitable candidate as structural materials for electrothermal microactuators. Furthermore, the performance enhancements in the electrothermal microactuator fabricated using Ni-diamond nanocomposite show the potential applications of the process for improving many MEMS devices, especially in terms of the characteristics of stronger mechanical strength and better electrical-to-mechanical energy conversion.

## ACKNOWLEDGMENT

The authors would like to express their appreciation to the Nano Facility Center of National Chiao Tung University, Prof. Fang in National Tsing Hua University and Prof. Pan in National Chin-Yi Technology for providing technical support and the measurement facilities.

## REFERENCES

[1] S. H. Lee, K. C. Lee, S. S. Lee, and H. S. Oh, "Fabrication of an electrothermally actuated electrostatic microgripper," in *Proc. 12th International Conference on Solid State Sensors, Actuators and Microsystems*, Boston, MA, 2003, pp. 552–555.

[2] P. M. Zavracky, S. Majumder, and N. E. McGruer, "Micromechanical switches fabricated using nickel surface micromachining," *J. Microelectromech. Syst.*, vol. 6, 1997.

[3] L. Li and L. Wang, "Micromanipulator system in MEMS," in *Proc. IEEE International Conference on Industrial Technology*, 1996, pp. 665–668.

[4] S. H. Lee, K. C. Lee, S. S. Lee, and H. S. Oh, "Fabrication of an electrothermally actuated electrostatic microgripper," in *Proc. 12th International Conference on Solid State Sensors, Actuators and Microsystems*, Boston, MA, 2003, pp. 552–555.

[5] J. Li, M. Kahrizi, and L. M. Landsberger, "Design, fabrication and characterization of CMOS—Compatible optical microswitches" (in Canadian), *IEEE Elect. Comput. Eng.*, pp. 319–322, 2003.

[6] K. K. Tan and S. C. Ng, "Computer-Controlled piezo micromanipulation system for biomedical applications," *Eng. Sci. Educ. J.*, pp. 249–256, 2001.

[7] J. B. Yoon, C. H. Han, E. Yoon, and C. K. Kim, "Monolithic integration of 3-D electroplated microstructures with unlimited number of levels using planarization with a sacrificial metallic mold (PSMM)," in *Proc. IEEE International Conference on Micro Electro Mechanical Systems*, 1999, pp. 624–629.

[8] J. Y. Park, G. H. Kim, K. W. Chung, and J. U. Bu, "Monolithically integrated micromachined RF MEMS capacitive switches," *Sens. Actuators A, Phys.*, vol. 89, pp. 88–94, 2001.

[9] C. P. Hsu, W. C. Tai, and W. Hsu, "Design and analysis of an electrothermally driven long-stretch micro drive with cascaded structure," in *Proc. 2002 ASME International Mechanical Engineering Congress & Exposition*, New Orleans, LA, 2002.

[10] Linder, L. Paratte, M. A. Gretillat, V. P. Jaeckin, and D N. F. Rooij, "Surface micromachining," *J. Micromech. Microeng.*, vol. 2, pp. 122–132, 1992.

[11] M. E. Mcnie, R. R. Davies, N. Price, D. O. King, and K. M. Brunson, "Advanced micromechanical prototyping in polysilicon and SOI," in *Proc. IEEE Seminar*, 2001.

[12] C. Hsu and W. Hsu, "Electrothermally-Driven long stretch micro drive with monolithic cascaded actuation units in compact arrangement," in *Proc. IEEE Transducers'03*, Boston, MA, 2003, pp. 8–12.

[13] H. Guckel, J. Klein, T. Christenson, K. Skrobis, M. Landon, and E. G. Lovell, "Thermo-Magnetic metal flexure actuators technical digest," in *Proc. IEEE Solid State Sensor and Actuator Workshop*, 1992, pp. 73–75.

[14] H. C. Nathanson and R. A. Wickstrom, "A resonant-gate silicon surface transistor with high-Q band-pass properties," *Appl. Phys. Lett.*, vol. 7, no. 4, pp. 84–86, 1965.

[15] L. Que, L. Otradovec, A. D. Oliver, and Y. B. Gianchandani, "Pulse and DC operation lifetimes of bent-beam electrothermal actuators," in *Proc. 14th IEEE International Conference on Micro Electro Mechanical Systems*, 2001, pp. 570–573.

[16] L. Que, J. S. Park, and Y. B. Gianchandani, "Bent-Beam electrothermal actuators-part 1: Single beam and cascaded devices," *J. Microelectromech. Syst.*, vol. 10, pp. 247–254, 2001.

[17] K. S. Teh, Y. T. Cheng, and L. W. Lin, "Nickel nano-composite film for MEMS applications," in *Proc. 12th International Conference on Solid State Sensors, Actuators and Microsystems*, Boston, MA, 2003, pp. 1534–1537.

[18] X. Li and B. Bhushan, "A review of nanoindentation continuous stiffness measurement technique and its applications," *Mater. Charact.*, vol. 48, pp. 11–36, 2002.

[19] S. Timoshenko, D. H. Young, and W. Weaver Jr, *Vibration Problems in Engineering*, 4th ed. New York: Wiley, 1974.

[20] H. V. Tasi, "Characterization of Mechanical Properties of Thin films Using Micromachined Structures," Ph.D., National Tsing Hua Univeristy, HsinChu, 2003.

[21] J. K. Luo, A. J. Flewitt, S. M. Spearing, N. A. Fleck, and W. I. Milne, "Young's modulus of electroplated ni thin film for MEMS applications," *Mater. Lett.*, vol. 58, pp. 2306–2309, 2004.
[22] C. S. Pan and W. S. Hsu, "An electro-thermally and laterally driven polysilicon microactuator," *J. Micromech. and Microeng.*, vol. 7, pp. 7–13, 1997.
[23] W. D. CallisterJr, *Materials Science and Engineering*, 3rd ed. New York: Wiley, 1994, pp. 516–521.
[24] G. E. Dieter, *Mechanical Metallurgy*, 3rd ed. New York: McGraw-Hill Book, 1978, pp. 184–240.
[25] J. P. Holman, *Heat Transfer*, 6th ed. New York: McGraw-Hill, 1989.
[26] C. S. Pan and W. S. Hsu, "A microstructure for in situ determination of residual strain," *J. Microelectromech. Syst.*, vol. 8, pp. 200–207, 1999.
[27] L. Lin and M. Chiao, "Electrothermal responses of lineshape microstructures," *Sens. Actuators A, Phys.* , vol. 55, pp. 35–41, 1996.
[28] L. Lin, A. P. Pisano, and V. P. Carey, "Thermal bubble formation on polysilicon micro resistors," *ASME J. Heat Transfer*, vol. 120, pp. 735–742, Sep. 1998.

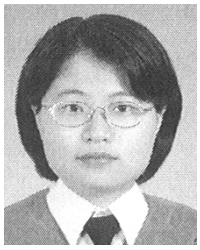

**Li-Nuan Tsai** was born in Taiwan, R.O.C. She received the B.S. and M.S. degree from the Da Yeh University, Chang-hua, Taiwan, R.O.C., in 1999 and 2002, respectively. Currently, she is working towards the Ph.D. degree in the Mechanical Engineering Department of Nation Chiao Tung University, working on MEMS design and fabrication process.

**Guang-Ren Shen** was born in Taiwan, Republic of China. He received the B.S. degree in physics from National Taiwan Normal University in 2002 and the M.S. degree in electrical engineering from National Chiao-Tung University in 2004. His thesis was the synthesis and characterization of Ni-P-CNT's and Ni-P-Diamond nanocomposite films for MEMS applications.

Currently, he works for BenQ as the engineer for the development of MEMS microfabrication.

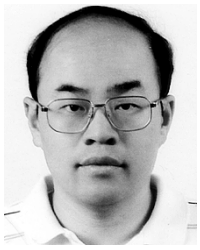

**Yu-Ting Cheng** (M'00) was born in Taiwan, Republic of China. He received the B.S. and M.S. degrees in materials science and engineering from National Tsing Hua University, Hsinchu, Taiwan, in 1991 and 1993, respectively. After serving his two-year army service in Taiwan, he went for Carnegie Mellon University, Pittsburgh, PA, and received the second M.S. degree in the same field. He received the Ph.D. degree in electrical engineering from the University of Michigan, Ann Arbor, in 2000. His dissertation is the development of novel vacuum packaging technique for MEMS applications.

After his graduation, he worked for IBM Watson Research Center, Yorktown Heights, NY, as a Research Staff Member and involved in several SoP (System on Package) projects. In 2002, he became an Assistant Professor at the Department of Electronics Engineering in National Chiao Tung University. His research interests include the fundamental study of materials for Microsystems integration and MEMS applications, SOP, and microsensors and microactuators.

Dr. Cheng is a member of IOP and Phi Tau Phi.

**Wensyang Hsu** received the M.S. and Ph.D. degrees in mechanical engineering from the University of California, Berkeley, in 1990 and 1992, respectively.

He is the Professor in Mechanical Engineering Department of National Chiao Tung University, Taiwan. His current interests include microactuators and metal-based surface micromachining.